Experimental Demonstration of Self-Guided Quantum Tomography

Robert J. Chapman,[1] Christopher Ferrie,[2] and Alberto Peruzzo[1,*]
[1]Quantum Photonics Laboratory, School of Engineering, RMIT University, Melbourne, Victoria 3000, Australia
and School of Physics, The University of Sydney, Sydney, New South Wales 2006, Australia
[2]Centre for Engineered Quantum Systems, School of Physics, The University of Sydney,
Sydney, New South Wales 2006, Australia
(Received 10 April 2016; published 21 July 2016)

Traditional methods of quantum state characterization are impractical for systems of more than a few qubits due to exponentially expensive postprocessing and data storage and lack robustness against errors and noise. Here, we experimentally demonstrate self-guided quantum tomography performed on polarization photonic qubits. The quantum state is iteratively learned by optimizing a projection measurement without any data storage or postprocessing. We experimentally demonstrate robustness against statistical noise and measurement errors on single-qubit and entangled two-qubit states.

DOI: 10.1103/PhysRevLett.117.040402

Quantum technologies require high-fidelity preparation, control, and characterization of quantum states, for application in quantum metrology [1], simulators [2], and computers [3]. Recent advances in the control of several qubits have enabled demonstrations of quantum error correction [4] and boson sampling [5,6]. Standard quantum tomography (SQT) has been the cornerstone of quantum state characterization for decades [7–9] and requires performing and storing data from an exponentially large number of projection measurements. Additionally, SQT has an exponential postprocessing cost to perform a state-estimation inverse problem which requires, for example, maximum likelihood estimation to avoid unphysical results. The scaling and additional postprocessing cost make SQT impractical for the size of quantum states being prepared today [10,11]. The reliability of SQT for all system sizes is limited by sensitivity to statistical noise and experimental errors. Unless modified at additional resource cost [12], SQT fails in the presence of measurement errors [13].

Adaptive quantum tomography (AQT) has demonstrated improved efficiency and precision by using state-dependent tomographic measurements [14–20]. AQT relies on solving an optimization problem using previous results to select the next measurement to be performed. As a result, AQT is as computationally expensive as SQT and likewise is sensitive to statistical noise and experimental errors.

Self-guided quantum tomography (SGQT) is an autonomous, robust, and precise method for characterizing quantum states [21]. Here, we demonstrate the performance and robustness of SGQT in several one- and two-qubit experiments. SGQT treats tomography as a projection measurement optimization problem using an iterative stochastic gradient ascent algorithm [22]. SGQT is therefore robust against both statistical noise and experimental errors, does not require the storage of exponentially large data sets, and does not require any data postprocessing. SGQT avoids many of the pitfalls of SQT and AQT at the small added cost in the number of different measurement settings required.

SGQT iteratively learns the quantum state through maximizing the expectation value of a projection measurement. The algorithm is graphically illustrated in Fig. 1. The unknown quantum state ρ_f is shown as a red Bloch vector, and the current estimate of the state at iteration k is $|\phi_k\rangle$, shown as a blue Bloch vector in Fig. 1(a). A direction Δ_k is chosen stochastically, and the expectation values of projectors $|\phi_k \pm \beta_k \Delta_k\rangle$ are measured, shown as green and purple Bloch vectors in Fig. 1(b). The expectation values are measured as

$$E(\rho_f, |\phi_k \pm \beta_k \Delta_k\rangle) = \langle \phi_k \pm \beta_k \Delta_k | \rho_f | \phi_k \pm \beta_k \Delta_k \rangle, \quad (1)$$

where $\beta_k = [b/(k+1)^t]$ controls the gradient estimation step size, with b and t as algorithm parameters. The expectation value gradient in the direction Δ_k is estimated as

$$g_k = \frac{E(\rho_f, |\phi_k + \beta_k \Delta_k\rangle) - E(\rho_f, |\phi_k - \beta_k \Delta_k\rangle)}{2\beta_k}. \quad (2)$$

Next, the estimate of the state is updated to $|\phi_{k+1}\rangle = |\phi_k + \alpha_k g_k \Delta_k\rangle$ in the direction of the highest expectation value, where $\alpha_k = [a/(k+1+A)^s]$ is the step size which decreases with iteration number k and A, a, and s are algorithm parameters. The state $|\phi_{k+1}\rangle$ is shown as a blue Bloch vector in Fig. 1(c), and this process is repeated until termination at a set number of iterations. The final estimate of the state is the final projection $|\phi_N\rangle$, where the number of iterations N is chosen from numerical simulation and experimental trials; however, in principle, one could predict the necessary number of iterations from the required fidelity, the size of the quantum system, and the level of noise. Here, we have not implemented such a method; however, it will

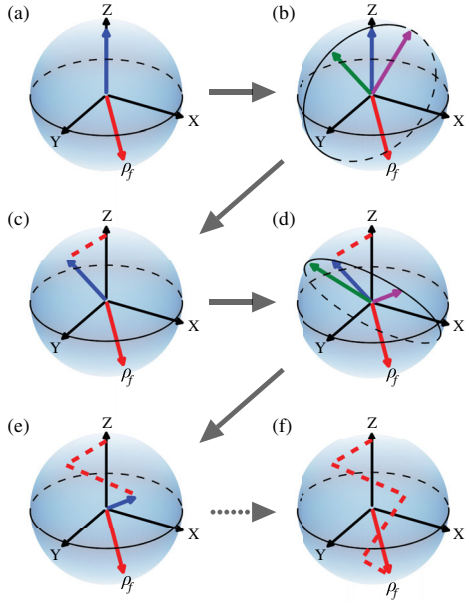

FIG. 1. (a) The unknown quantum state that we want to characterize is shown as a red Bloch vector, and the current estimation is shown as a blue Bloch vector. (b) The algorithm estimates the gradient in a stochastically chosen direction by performing expectation value measurements with the green and purple projectors. (c) The algorithm steps in the direction of the highest expectation value, and the current estimate of the state is updated. (d)–(f) The gradient is estimated again and the process repeated for a set number of iterations.

be included in future work. The algorithm parameters A, a, b, s, and t can be asymptotically optimized off-line. The asymptotically optimal values are $s = 1$ and $t = 1/6$; however, it was often found that $s = 0.602$ and $t = 0.101$ performed well. In general, the other parameters we kept as $a = 3$, $b = 0.1$, and $A = 0$. The algorithm is robust against noisy gradient estimates, and, as such, SGQT is robust against statistical noise and measurement errors.

We experimentally demonstrate SGQT using polarization encoded photonic qubits. We generate pairs of indistinguishable photons from a spontaneous parametric down-conversion source [23] and prepare heralded single-qubit and entangled two-qubit states using motor-controlled rotating wave plates. Projection onto any one- or two-qubit separable state is implemented using further motor-controlled wave plates and polarizing beam splitters (see Supplemental Material [24] for full experimental details). We calculate the expectation value in Eq. (1) by measuring the number of photons recorded as a proportion of the total photon flux for a fixed integration time.

We first demonstrate the robustness of one-qubit SGQT against statistical noise by reducing our photon count rate such that, with the minimum integration time, we use on average seven photons per iteration of the algorithm. In this regime, Poissonian noise on the photon count is very high [25]. We perform SGQT on three target states using the minimum integration time and repeat each run ten times. On the same target states, we perform SQT with a range of integration times to control the total number of photons used, repeating each measurement ten times.

In order to benchmark our results, we obtain a high-precision estimate of the target state using SQT with a high count rate and long integration time to reduce Poissonian noise. The total photon count is $\sim 2 \times 10^5$, and we calculate an expected precision of $99.9\% \pm 0.1\%$. To benchmark the performance of SGQT and SQT with a low photon count rate, we calculated the fidelity to this high-precision estimate [26]. We emphasize that we do not expect to see optimal convergence in the fidelity to the benchmark state, since our estimate is converging toward the true physical state.

Figure 2(a) shows the route of one SGQT run for each target state plotted on the Bloch sphere. We set the starting estimate to be $|0\rangle$, but this can be any state. Figure 2(b) shows a log-log plot with the fidelity of SGQT and SQT against the number of photons used. The red, green, and purple points are the average fidelity of SGQT for each target state. The red line is the average fidelity across all target states, and the band gives one standard deviation of error. The blue dots are the average fidelity of SQT across all target states. SQT on one qubit requires four measurements, and therefore a minimum of 28 photons are used. For all points, SGQT records a greater fidelity than SQT, demonstrating enhanced robustness against high levels of statistical noise. At the final iteration after ~280 photons have been used, SGQT achieves a fidelity of $99.3\% \pm 0.2\%$, whereas SQT records a fidelity of $96.7\% \pm 0.6\%$. To reach the same fidelity, SQT requires an order of magnitude more photons. Figure 2(c) shows a table comparing fidelity against number of photons used for SGQT and SQT. In a high noise regime, this result demonstrates that SGQT is far more resource efficient than SQT.

To compare robustness against one-qubit measurement errors, we perform SGQT and SQT in a regime where we have a large uncertainty in the projection measurement. We engineer this level of uncertainty by applying random errors to the wave plate settings. SQT and AQT require high precision of each projection measurement setting, whereas SGQT is robust against independent measurement errors. We apply four levels of wave plate uncertainty, perform SGQT and SQT ten times each, and measure the average fidelities, again benchmarked against long integration SQT without applied errors.

Figure 3 presents the average fidelity of SGQT and SQT for each level of error. The results show that SGQT outperforms SQT after only ~10 iterations, and after 40 iterations the infidelity [1-fidelity (F)] of SGQT is up to 89% lower than SQT, calculated as $[(F_{\mathrm{SGQT}} - F_{\mathrm{SQT}})/(1 - F_{\mathrm{SQT}})]$, and will continue to decrease as numerically studied in Ref. [21]. These results demonstrate the robustness of SGQT to significant measurement errors. For this demonstration,

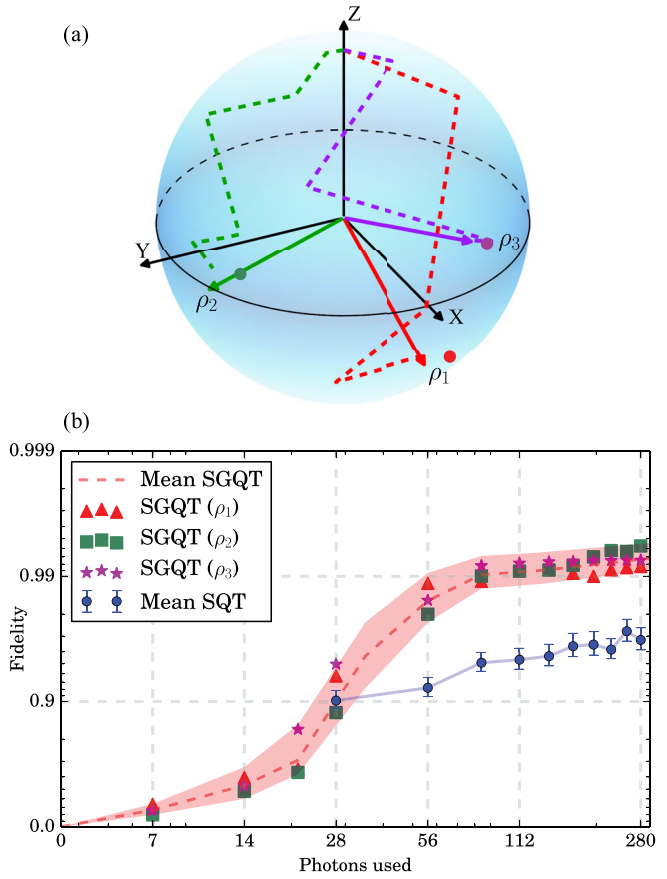

(c)

Method	Photon count	Fidelity
SQT	$\sim 2\text{x}10^5$	$99.9 \pm 0.1\%$
SQT	$\sim 3.9\text{x}10^3$	$99.5 \pm 0.7\%$
SQT	~ 280	$96.7 \pm 0.6\%$
SGQT	~ 280	$99.3 \pm 0.2\%$

FIG. 2. We perform SGQT in a regime where only seven photons on average are used per iteration of the algorithm. (a) A single SGQT route for each target state is plotted on the Bloch sphere. (b) The red, green, and purple points show the average fidelity of SGQT for each target state. The red line shows the average fidelity across all target states. The blue points show the average fidelity of SQT across all target states for different total photon counts. (c) The table compares the fidelity of SGQT with ~280 photons to SQT with ~280, $\sim 3.9 \times 10^3$ and $\sim 2 \times 10^5$ photons used.

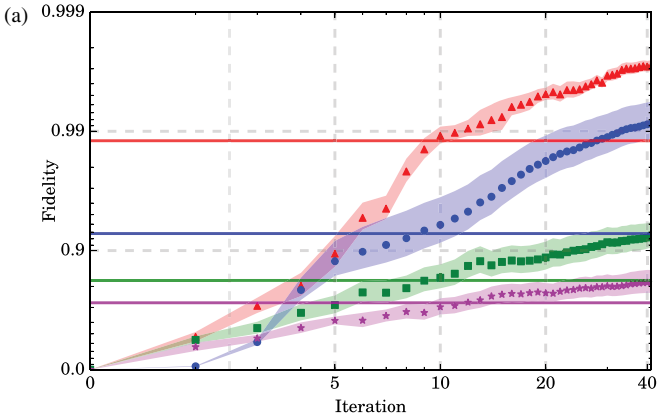

(b)

SQT 40 measurements (10 repeats)	SGQT 40 iterations
$98.8 \pm 0.5\%$	$99.72 \pm 0.03\%$
$92.8 \pm 1.2\%$	$99.2 \pm 0.3\%$
$82.2 \pm 3.5\%$	$92.5 \pm 1.8\%$
$72.6 \pm 4.6\%$	$81.1 \pm 4.0\%$

FIG. 3. (a) Fidelity of SGQT with varying levels of experimental error. Points are the average of ten repetitions, and the band gives one standard deviation of error. SQT is performed with the same levels of experimental error, repeated ten times, and the fidelities shown as solid lines. (b) Table comparing the fidelity values for SQT after ten repetitions (40 measurements) and SGQT after 40 iterations.

we reduce statistical noise by increasing the photon count rate to $\sim 5 \times 10^3$ per iteration; however, in the presence of both significant statistical noise and measurement errors, SGQT will still converge with high fidelity.

Extending SGQT to a greater number of qubits simply requires a parametrization of the projection measurement, which the algorithm can optimize to find the maximum overlap with the physical state. In order to be universal, the algorithm requires any projection measurement, including entangling measurements, to estimate the gradient from Eqs. (1) and (2) [21]. We next demonstrate the performance and robustness of SGQT to characterize a two-qubit entangled state. However, in this experiment we use only local measurements which are available in our setup, and, therefore, we cannot use the expectation value calculated in Eq. (1) to estimate the gradient. Instead, we perform a subset of Pauli measurement M at each iteration of the algorithm, which is insufficient for SQT but gives partial knowledge of the target state ρ_f from which we calculate the fidelity to the current estimate of the state $|\Phi_k\rangle$ as

$$\tilde{F}(\rho_f, |\Phi_k\rangle) = \frac{1}{|M|} \sum_{i \in \{M\}} \frac{\mathrm{Tr}(\rho_f P_i^{(2)})}{\langle \Phi_k | P_i^{(2)} | \Phi_k \rangle}, \tag{3}$$

where $|M|$ is the number of Pauli measurements per iteration and $P^{(2)} = \{\sigma_I \otimes \sigma_I, \sigma_I \otimes \sigma_X, \sigma_I \otimes \sigma_Y, \ldots, \sigma_Z \otimes \sigma_Z\}$ are the two-qubit Pauli matrices [27,28]. $\tilde{F}(\rho_f, \cdot)$ replaces $E(\rho_f, \cdot)$ in Eq. (2) to estimate the gradient. In this context, existing AQT techniques would select measurements based on the solution of an optimization problem, whereas SGQT selects a random set of measurements at each iteration and is thus much more computationally efficient.

We experimentally demonstrate SGQT on a two-qubit maximally entangled Bell state $|\Psi^-\rangle = 1/\sqrt{2}(|01\rangle - |10\rangle)$. We run the algorithm taking a random subset of Pauli measurements per iteration. Figure 4 presents the results of

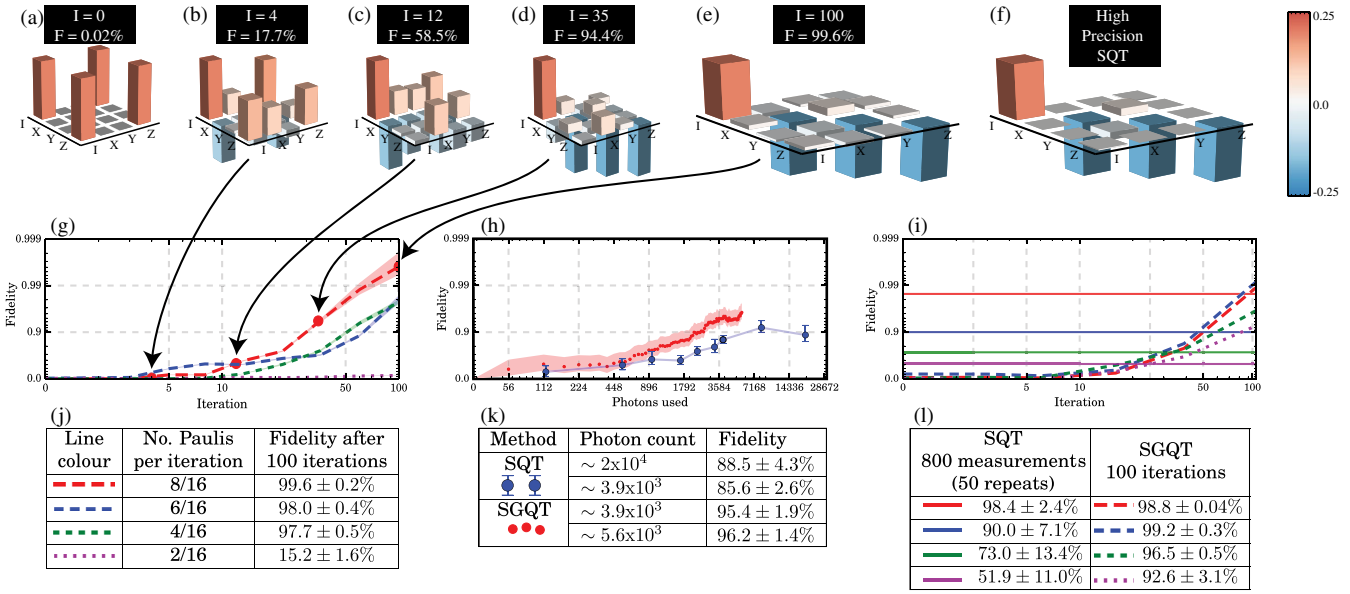

(j)

Line colour	No. Paulis per iteration	Fidelity after 100 iterations
	8/16	$99.6 \pm 0.2\%$
	6/16	$98.0 \pm 0.4\%$
	4/16	$97.7 \pm 0.5\%$
	2/16	$15.2 \pm 1.6\%$

(k)

Method	Photon count	Fidelity
SQT	$\sim 2\text{x}10^4$	$88.5 \pm 4.3\%$
	$\sim 3.9\text{x}10^3$	$85.6 \pm 2.6\%$
SGQT	$\sim 3.9\text{x}10^3$	$95.4 \pm 1.9\%$
	$\sim 5.6\text{x}10^3$	$96.2 \pm 1.4\%$

(l)

SQT 800 measurements (50 repeats)	SGQT 100 iterations
$98.4 \pm 2.4\%$	$98.8 \pm 0.04\%$
$90.0 \pm 7.1\%$	$99.2 \pm 0.3\%$
$73.0 \pm 13.4\%$	$96.5 \pm 0.5\%$
$51.9 \pm 11.0\%$	$92.6 \pm 3.1\%$

FIG. 4. We perform SGQT on two-qubit states by taking a random subset of Pauli measurements at each iteration. We present the state in terms of Pauli measurement expectation values, where element $i, j = \frac{1}{4}\langle\Phi_k|P_i^{(1)} \otimes P_j^{(1)}|\Phi_k\rangle$ and $P^{(1)} = \{\sigma_I, \sigma_X, \sigma_Y, \sigma_Z\}$ are the one-qubit Pauli matrices. (a)–(e) The estimate of the state at different points of the algorithm run with eight measurements per iteration. The fidelity is measured against high-precision SQT. (f) The high-precision estimate of the state measured with SQT using a long integration time to reduce statistical noise. (g) The algorithm was run with eight, six, four, and two measurements per iteration, and the fidelity of the state estimate is plotted. The table below compares fidelities. (h) We compare performance of SGQT and SQT in the presence of high levels of statistical noise and measure the fidelity against the number of photons used. (i) We engineer measurement errors in wave plate rotations and measure the fidelity of SGQT and SQT with four levels of error. We repeat SQT to match the number of measurements of SGQT and average the results. Both (h) and (i) use eight measurements per iteration.

the algorithm. Figures 4(a)–4(e) show the state estimate throughout the algorithm using eight measurements per iteration, presented as Pauli measurement expectation values. Figure 4(f) shows the target state as measured with long integration SQT, and the fidelity to the final SGQT estimate is $99.6\% \pm 0.2\%$. Figure 4(g) presents the fidelity of SGQT against the iteration number for a range of measurements per iteration. It is clear that with eight, six, and four measurements per iteration (red, blue, and green lines, respectively) the algorithm converges with high fidelity after 100 iterations; however, with two Pauli measurements per iteration the algorithm appears not to converge, which could be a result of an insufficient number of iterations or insufficient fidelity precision from Eq. (3). Figure 4(j) presents the final fidelities.

We demonstrate the robustness of two-qubit SGQT against statistical noise by again reducing the photon count rate to a regime where on average seven photons are used per measurement. We also perform SQT using an equivalent total number of photons to allow direct resource comparison. Figure 4(h) presents the fidelity of SGQT where eight measurements are used per iteration and SQT using the same total number of photons. SGQT achieves 68% lower infidelity than SQT, which again requires around an order of magnitude more photons to achieve the same level of fidelity. The fidelity values are presented in Fig. 4(k), demonstrating enhanced robustness of two-qubit SGQT while using only local measurements.

We finally investigate the robustness against measurement errors on two-qubit SGQT by applying wave plate uncertainty. With the same four levels of error as the one-qubit case, we perform SGQT and SQT on the entangled Bell state. Figure 4(i) presents the fidelity of SGQT against the iteration number with the experimental error applied. SQT is repeated with the same total number of measurements and the results averaged. The SQT fidelities are plotted in Fig. 4(i) as horizontal lines for each level of error. Using the same total number of measurements, SGQT achieves up to a 92% lower infidelity than SQT, presented in Fig. 4(l).

We have demonstrated the advantages of SGQT over standard techniques for characterizing quantum states in a range of one- and two-qubit experiments. In experiments where there is a high level of noise or large experimental error, SGQT is shown to achieve higher fidelity than with SQT measurements alone on both single-qubit and two-qubit entangled states. This method requires only local projection measurements; however, if entangling projections are available, then the original form of the algorithm can be used. In our implementation, the algorithm finds the pure state with the greatest overlap to the physical state. In the single-qubit case, the purity can be calculated by

comparing the photon count at the final projection to the photon count with an orthogonal projection. While, in this experiment, the states we prepare are highly pure and this additional step is unnecessary to achieve high fidelity, future work will report on extending this technique to larger systems and demonstrate the performance of SGQT on arbitrary mixed states.

While the cost of SGQT is still exponential with the system size in the number of measurements, it does not require data storage or computationally expensive post-processing and maximum likelihood estimation to characterize an unknown quantum state. This algorithm can also be applied to state preparation and quantum device control [29]. SGQT opens future pathways toward robust characterization of quantum systems with dimensions where standard tomographic techniques have already become impractical.

We thank Chad Husko for providing technical support. C. F. was supported by the U.S. Army Research Office Grants No. W911NF-14-1-0098 and No. W911NF-14-1-0103 and by the Australian Research Council Centre of Excellence for Engineered Quantum Systems, Project No. CE11001013. A. P. acknowledges an Australian Research Council Discovery Early Career Researcher Award, Project No. DE140101700 and an RMIT University Vice-Chancellor's Senior Research Fellowship.

*alberto.peruzzo@rmit.edu.au

[1] V. Giovannetti, S. Lloyd, and L. Maccone, Nat. Photonics **5**, 222 (2011).
[2] S. Lloyd, Science **273**, 1073 (1996).
[3] T. D. Ladd, F. Jelezko, R. Laflamme, Y. Nakamura, C. Monroe, and J. L. OBrien, Nature (London) **464**, 45 (2010).
[4] D. Nigg, M. Müller, E. A. Martinez, P. Schindler, M. Hennrich, T. Monz, M. A. Martin-Delgado, and R. Blatt, Science **345**, 302 (2014).
[5] M. A. Broome, A. Fedrizzi, S. Rahimi-Keshari, J. Dove, S. Aaronson, T. C. Ralph, and A. G. White, Science **339**, 794 (2013).
[6] J. B. Spring, B. J. Metcalf, P. C. Humphreys, W. S. Kolthammer, X.-M. Jin, M. Barbieri, A. Datta, N. Thomas-Peter, N. K. Langford, D. Kundys, J. C. Gates, B. J. Smith, P. G. R. Smith, and I. A. Walmsley, Science **339**, 798 (2013).
[7] G. G. Stokes, Trans. Cambridge Philos. Soc. **9**, 399 (1851).
[8] U. Fano, Rev. Mod. Phys. **29**, 74 (1957).
[9] K. Banaszek, M. Cramer, and D. Gross, New J. Phys. **15**, 125020 (2013).
[10] B. Vlastakis, G. Kirchmair, Z. Leghtas, S. E. Nigg, L. Frunzio, S. M. Girvin, M. Mirrahimi, M. H. Devoret, and R. J. Schoelkopf, Science **342**, 607 (2013).
[11] F. Haas, J. Volz, R. Gehr, J. Reichel, and J. Estve, Science **344**, 180 (2014).
[12] A. M. Braczyk, D. H. Mahler, L. A. Rozema, A. Darabi, A. M. Steinberg, and D. F. V. James, New J. Phys. **14**, 085003 (2012).
[13] S. J. v. Enk and R. Blume-Kohout, New J. Phys. **15**, 025024 (2013).
[14] D. G. Fischer, S. H. Kienle, and M. Freyberger, Phys. Rev. A **61**, 032306 (2000).
[15] F. Huszar and N. M. T. Houlsby, Phys. Rev. A **85**, 052120 (2012).
[16] T. Hannemann, D. Reiss, C. Balzer, W. Neuhauser, P. E. Toschek, and C. Wunderlich, Phys. Rev. A **65**, 050303 (2002).
[17] D. H. Mahler, L. A. Rozema, A. Darabi, C. Ferrie, R. Blume-Kohout, and A. M. Steinberg, Phys. Rev. Lett. **111**, 183601 (2013).
[18] K. S. Kravtsov, S. S. Straupe, I. V. Radchenko, N. M. T. Houlsby, F. Huszar, and S. P. Kulik, Phys. Rev. A **87**, 062122 (2013).
[19] G. Struchalin, I. Pogorelov, S. Straupe, K. Kravtsov, I. Radchenko, and S. Kulik, Phys. Rev. A **93**, 012103 (2016).
[20] B. Qi, Z. Hou, Y. Wang, D. Dong, H.-S. Zhong, L. Li, G.-Y. Xiang, H. M. Wiseman, C.-F. Li, and G.-C. Guo, arXiv:1512.01634.
[21] C. Ferrie, Phys. Rev. Lett. **113**, 190404 (2014).
[22] J. Spall, IEEE Trans. Autom. Control **37**, 332 (1992).
[23] D. C. Burnham and D. L. Weinberg, Phys. Rev. Lett. **25**, 84 (1970).
[24] See Supplemental Material at http://link.aps.org/supplemental/10.1103/PhysRevLett.117.040402 for full details of the polarization photonic experiment.
[25] R. J. Glauber, Phys. Rev. Lett. **10**, 84 (1963).
[26] M. A. Nielsen and I. L. Chuang, *Quantum Computation and Quantum Information*, 10th ed. (Cambridge University Press, Cambridge, England, 2010).
[27] S. T. Flammia and Y.-K. Liu, Phys. Rev. Lett. **106**, 230501 (2011).
[28] M. P. da Silva, O. Landon-Cardinal, and D. Poulin, Phys. Rev. Lett. **107**, 210404 (2011).
[29] C. Ferrie and O. Moussa, Phys. Rev. A **91**, 052306 (2015).